2024 IEEE International Conference on Robotics and Automation (ICRA 2024)
May 13-17, 2024. Yokohama, Japan

Force-based semantic representation and estimation of feature points for robotic cable manipulation with environmental contacts

Andrea Monguzzi[1], Yiannis Karayiannidis[2], Paolo Rocco[1], Andrea Maria Zanchettin[1]

***Abstract*— This work demonstrates the utility of dual-arm robots with dual-wrist force-torque sensors in manipulating a Deformable Linear Object (DLO) within an unknown environment that imposes constraints on the DLO's movement through contacts and fixtures. We propose a strategy to estimate the pose of unknown environmental contacts encountered during the manipulation of a DLO, classifying the induced constraints as *unilateral, bilateral* and *fully constrained*, exploiting the redundancy of force sensors. A semantic approach to define environmental constraints is introduced and incorporated into a graph-based model of the DLO. This model remains accurate as long as the DLO is under tension and is dynamically updated throughout the manipulation process, built by sequencing a set of primitives. The estimation strategy is validated through simulations and real-world experiments, demonstrating its potential in handling DLOs under various, possibly uncertain, constraints.**

I. Introduction

The robotic manipulation of Deformable Linear Objects (DLOs) (such as cables, wires, and ropes) is common in several industrial tasks and leads to many interesting open challenges [1]. DLOs can be classified into two categories [2]: objects with no or low compression strength and elements that exhibit large strain during manipulation. This work addresses DLOs in the first category that oppose resistance to deformation and transmit forces only if taut. The manipulation of such DLOs can be simplified by keeping them under tension and exploiting environmental contacts to constrain some of their degrees of freedom (DoFs), achieving a desired shape [3], [4]. Strategies to route stiff DLOs exploiting environmental constraints are also analysed [5]. To execute assembly operations, it is essential to estimate the current state of the DLO in relation to the possibly unknown or uncertain environment. For instance, when routing a cable, the class (*unilateral* or *bilateral*) and the location of constraints imposed by the environment must be identified. Similarly, when disconnecting DLO ends [6], the position of the fixtures *fully constraining* them has to be estimated.

[1]A. Monguzzi, P. Rocco, A. M. Zanchettin are with Politecnico di Milano, Dipartimento di Elettronica, Informazione e Bioingegneria (DEIB), Piazza Leonardo da Vinci 32, 20133, Milano (Italy). e-mail: {andrea.monguzzi, paolo.rocco, andreamaria.zanchettin}@polimi.it

[2] Y. Karayiannidis is with the Department of Automatic Control, LTH, Lund University, SE-221 00 Lund (Sweden). The author is a member of the ELLIIT Strategic Research Area at Lund University. e-mail: yiannis.@control.lth.se

This work was supported by Progetto Prin 2020 "Co-Mir", prot. 2020CMEFPK and partially supported by "WASP" funded by the Knut and Alice Wallenberg Foundation.

The authors acknowledge Gabriel Arslan Waltersson and Rita Laezza's help during the preparation of the robotic setup used.

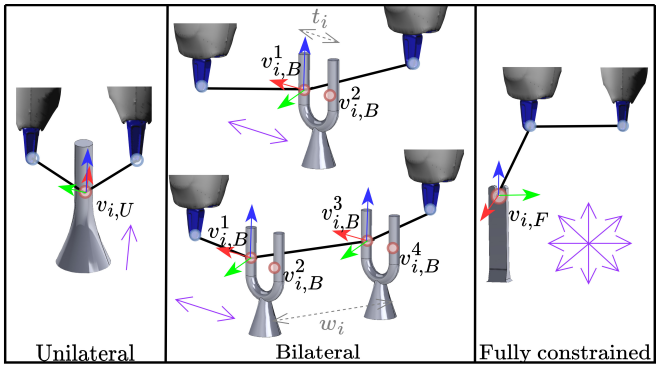

Fig. 1: A constraint is defined by one or more feature points $v_{i,S}$ where $S \in \{U, B, F\}$ (in red), each one characterized by a position and a frame, allowing to define the DLO shape. Frames of $v^2_{i,B}$, $v^4_{i,B}$ are omitted for the sake of readability. The constrained directions of motion are depicted in purple.

In this work, we consider a dual-arm robot, equipped with two wrist force torque (FT) sensors, that manipulates a DLO. The operation is performed in an unknown environment, that imposes constraints during the manipulation. The use of a dual-arm robot and the information acquired from the two FT sensors are instrumental in extending the state representation of the manipulated DLO kept under tension. We formally describe environmental constraints with a semantic representation that is embedded in a path graph model describing the DLO's shape as a set of feature points, enhancing the DLO model described in [7]. The constraints are classified as *unilateral*, *bilateral*, or *fully constrained*: Figure 1 shows the proposed semantic representation that enables the robotic understanding of the workspace. During the DLO manipulation, achieved via six implemented primitives, the environmental contacts are classified, depending on the generated constraints, and their poses are estimated through force-position based estimators. To the best of our knowledge, the benefits of using two FT sensors for the manipulation of a DLO in a constrained environment have not yet been addressed in the literature.

The rest of this work is organised as follows. Section II reviews the related works, emphasizing contributions. Section III presents the enhanced DLO graph model, while Section IV defines the estimators used. Sections V and VI detail the manipulation primitives and the pipeline for classifying and estimating feature points. Section VII discusses the experimental validation, and Section VIII concludes the paper.

II. Related works and contributions

Force-based estimation of rigid objects' features or environmental contacts is extensively studied in the literature. For

example, [8] exploits a FT sensor on the flange of a dual-arm robot to estimate the joint location and direction of a manipulated two DOFs object, while in [9] a dual-arm robot with two FT sensors is used to estimate the center of mass of a rigid tray with objects. [10] presents an algorithm to detect external contacts on the robot body exploiting the measured joint torques. [11] proposes a Bayesian state estimator for manipulation tasks characterized by contacts, such as nonprehensile manipulation. As stated in [12], most of the robotized tasks exploiting force manipulation in contacts involve stiff objects, while few works deal with Deformable Objects (DOs) as deformation leads to a complex description of the physics characterizing the task and requires complex state representations. Focusing on robotic interaction with DOs, [13] and [14] analyse robot contact tasks in the presence of deformable surfaces. However, few works in the literature deal with contact estimation in DLO robotic manipulation. [15] and [16] deal with force-based detection of contact state transitions between a DLO and the environment, while in [4] contacts between a DLO and pegs are detected using a vision-based strategy. The authors of [17] propose a strategy to learn the dynamics of a graph model for DLO with external contacts based on visual information, using them to define a control action to drive the DLO to a desired shape. Contact estimation for a manipulated DLO using a force-based approach is presented in [7], where a dual-arm robot equipped with one FT sensor is considered. In [7], a graph model describing the shape of the DLO as a set of feature points was proposed incorporating estimates of the contacts without however classifying them. FT sensing has also been exploited for the manipulation of DOs [18]–[20] without environmental interaction, for example, to define inputs for physical DLOs models [21], [22], to plan a collision-free path [23], or to perform contour following [24].

The main contributions of our method can be identified as:

1) A graph model is used to describe the shape of the DLO as a set of feature points based on force information instead of visual ones, in contrast to [17]. In particular, we enrich the model proposed in [7]: while in [7] a feature point can represent a gripper or a generic contact, we introduce a semantic classification of the feature points allowing to discriminate the kind of environmental constraint among *unilateral*, *bilateral* and *fully constrained*.

2) We consider a dual-arm robot equipped with two wrist FT sensors as in [9], but we address a different task as we deal with the manipulation of DLOs rather than rigid elements. The use of two FT sensors brings benefits allowing the estimation of *unilateral* and *bilateral* constraints without the need for wide motions around the contacts. This improves the strategy presented in [7], where generic contact points are estimated exploiting only one FT sensor requiring large motion, and enables the characterization of a *fully constrained* DLO end in a configuration that cannot be addressed with only one force measurement. Moreover, the use of two FT sensors enables a more comprehensive modelling of the tension along the DLO compared to the model of [7].

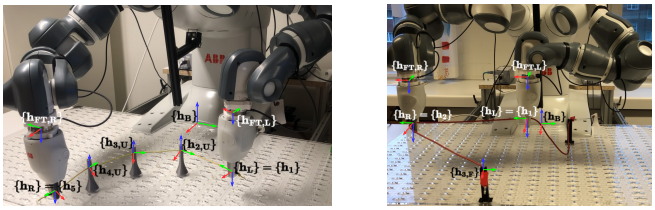

(a) (b)

Fig. 2: Considered setup and examples of environment: (a) *unilateral constraints*, (b) *fully constrained* ends. Relevant frames are highlighted. x, y, z axes are depicted in red, green and blue, respectively.

III. DLO PATH GRAPH MODEL WITH SEMANTIC REPRESENTATION OF FEATURE POINTS

This Section details the assumptions made in this work and the improvements made to the model of [7].

We consider a robot that has already grasped a DLO, knowing if it is initially grasping the ends or not. The pose of the feature points corresponding to the grippers is known, assuming no slipping of the DLO inside the fingertips. Figure 2 shows the setup considered in this work. Given that DLO and peg diameters are comparable, the contact surface is approximated as a contact point, where the static friction coefficient μ is assumed low (DLOs with plastic coating and metal pegs: $\mu \approx 0.1$). In the following, we indicate with $\{\mathbf{h}\}$ a generic reference frame and with ${}^{A}\mathbf{w}$ the vector $\mathbf{w}$ expressed in the reference frame $\{\mathbf{h}_A\}$; if no superscript is indicated, $\mathbf{w}$ is expressed in the base frame $\{\mathbf{h}_B\}$.

To model a uniformly weighted DLO, characterized by a weight per unit length ρ, we adopt the reduced graph model $\{\mathcal{G}, \rho\}$ proposed in [7]. The state of the DLO is modelled as a linear graph $\mathcal{G} = (V, E)$ where V is a set of feature points v_i, $i = 1, \dots, |V|$ and E is a set of edges e_i, $i = 1, \dots, |V| - 1$ connecting two adjacent feature points v_i and v_{i+1}.

A. Feature points: grippers and environmental constraints

A feature point is defined as $v_i = (\mathbf{p}_i, \mathbf{Q}_i, m_i)$, where $\mathbf{p}_i \in \mathbb{R}^3$ and the unit quaternion $\mathbf{Q}_i$ represent its position and the orientation of a frame attached to the point, respectively. m_i is the mass assigned considering an equal distribution of the DLO mass among the v_i. In [7], a feature point can represent a gripper, a generic contact with the environment or a user-defined point. We extend the definition of feature point proposing a semantic representation of the constraints. This is specified by an additional subscript S for each feature point, obtaining $v_{i,S}$, with S assuming values in the set $\{G, U, B, F\}$ depending on the nature of the constraints (*gripper, unilateral, bilateral, fully constrained*). In particular, feature points can represent:

I) Grippers holding the DLO. Each gripper is defined as a $v_{i,G}$ with $\mathbf{p}_i, \mathbf{Q}_i$ obtained by forward kinematics.

II) Environmental constraints (see Figure 1), classified as:

• *Unilateral* constraint, as the one generated by a peg that blocks only one direction of motion. It is represented by a feature point $v_{i,U}$ characterized by a position vector $\mathbf{p}_i$ that has to be estimated (Section VI) and a quaternion $\mathbf{Q}_i$, which together characterize frame $\{\mathbf{h}_{i,U}\}$. The x axis of $\{\mathbf{h}_{i,U}\}$

indicates the constrained direction of motion and is defined considering the two adjacent feature points to $v_{i,U}$. If v_{i-1} and v_{i+1} represent grippers, as in Figure 1, the unit vector $\boldsymbol{\chi}_i$ for the x axis of $\{\mathbf{h}_{i,U}\}$ is: $\boldsymbol{\chi}_i = (\dot{\mathbf{x}}_R + \dot{\mathbf{x}}_L)/||\dot{\mathbf{x}}_R + \dot{\mathbf{x}}_L||_2$, where $\dot{\mathbf{x}}_R$ and $\dot{\mathbf{x}}_L$ are the linear velocities of the TCPs when the contact is detected. Otherwise, if only one feature point describes a gripper (e.g. v_{i+1} is the left gripper), then $\boldsymbol{\chi}_i = (\boldsymbol{\chi}_{i-1} + \dot{\bar{\mathbf{x}}}_L)/||\boldsymbol{\chi}_{i-1} + \dot{\bar{\mathbf{x}}}_L||_2$, where $\dot{\bar{\mathbf{x}}}_L = \dot{\mathbf{x}}_L/||\dot{\mathbf{x}}_L||_2$, and $\boldsymbol{\chi}_{i-1}$ is the unit vector of the x axis of the frame linked to v_{i-1}. Finally, the z axis of $\{\mathbf{h}_{i,U}\}$ has the same orientation as the z axis of $\{\mathbf{h}_B\}$ and the y axis completes a right-handed frame.

• *Bilateral* constraint, generated by one peg hook or two pegs hook, constraining the motion from two sides. In the first case, the constraint is represented by two feature points $v^j_{i,B}$, $j = 1, 2$, while in the second one by four $v^j_{i,B}$, $j = 1, \dots, 4$. Each $v^j_{i,B}$ is characterized by an estimated position $\mathbf{p}^j_i$ and by a frame $\{\mathbf{h}^j_{i,B}\}$ (centered in $\mathbf{p}^j_i$) whose x axis is along one of the constrained directions of motion. In particular, considering $v^k_{i,B}$ and $v^s_{i,B}$ with $(k, s) \in \{(1, 2), (3, 4)\}$ (see Figure 1), it holds $\boldsymbol{\chi}_i = (\mathbf{p}^k_i - \mathbf{p}^s_i)/||\mathbf{p}^k_i - \mathbf{p}^s_i||_2$. The z axis has the same orientation as the one of $\{\mathbf{h}_B\}$, and the y axis completes a right-handed frame. Furthermore, two extra fields are added to the definition of $v^j_{i,B}$ detailing the thickness $t_i = ||\mathbf{p}^k_i - \mathbf{p}^s_i||_2$, $(k, s) \in \{(1, 2), (3, 4)\}$, and the width $w_i = ||\mathbf{p}^k_i - \mathbf{p}^s_i||_2$, $(k, s) \in \{(1, 3), (2, 4)\}$. t_i and w_i are highlighted in Figure 1. To represent a *bilateral* constraint, multiple feature points $v^j_{i,B}$ are needed, but they are not all linked by edges. The $v^j_{i,B}$ linked to v_{i-1} and v_{i+1} is the one whose $\mathbf{p}^j_i$ is currently being estimated. If $w_i \neq 0$, the $v^j_{i,B}$ estimated immediately before is linked as well.

• *Fully constrained*, generated by a fixture blocking all the DoFs of the DLO portion inserted. This constraint is represented by a $v_{i,F}$ described by an estimated $\mathbf{p}_i$ and by a $\{\mathbf{h}_{i,F}\}$ with same orientation of $\{\mathbf{h}_B\}$ and origin in $\mathbf{p}_i$.

Once a new contact is detected, its classification as *unilateral* constraint, part of a *bilateral* one or *fully constrained* and the estimation of its parameters are accomplished as detailed in Section VI. Every time a contact is detected, a new v_i is added to the graph and the indices are updated.

B. Edges: tension along the DLO

Each edge e_i is defined as $e_i = (d_i, s_i, f_i, k_i)$, where $d_i = ||\mathbf{p}_{i+1} - \mathbf{p}_i||_2$, $s_i \in \mathbb{R}$ is the sag, $f_i \in \mathbb{R}$ is the weight compensated tension along e_i and $k_i \in \mathbb{R}$ is an estimation of elasticity of the DLO along e_i. s_i (see [7] for detailed computation) allows assessing the assumption of a linear connection between v_i and v_{i+1}: if $s_i > \bar{s}$ ($\bar{s}$ is a user-defined threshold) d_i is not reliable and the tension along e_i has to be increased. If v_i represents an end effector (EE) equipped with a FT sensor, f_i is computed as in [7]:

$$\mathbf{u}_i f_i = \mathbf{f}_{sens} - \mathbf{g} m_i + \mathbf{u}_{i-1} f_{i-1} \tag{1}$$

where $\mathbf{u}_i = (\mathbf{p}_{i+1} - \mathbf{p}_i)/||\mathbf{p}_{i+1} - \mathbf{p}_i||_2$, $\mathbf{f}_{sens}$ denotes the force measurement, and $\mathbf{g}$ is the gravity acceleration.

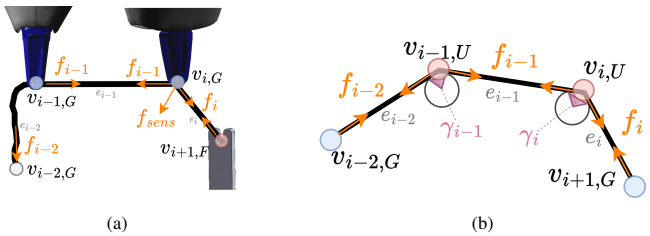

Fig. 3: (a) DLO with a *fully constrained* end $v_{i+1,F}$. v_{i-2} represent a free hanging point. (b) Routing of a DLO around pegs with contacts $v_{i-1,U}$, $v_{i,U}$. γ_{i-1}, γ_i are contact angles.

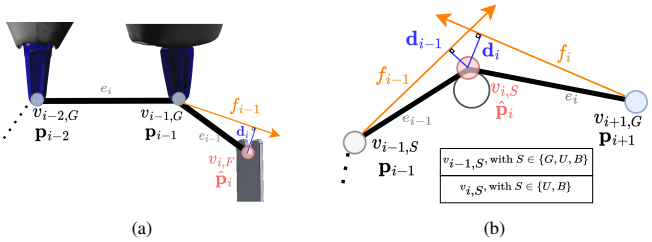

Fig. 4: Estimation of $\hat{\mathbf{p}}_i$ in case of (a) *fully constrained* DLO end and (b) single peg belonging to *unilateral* or *bilateral* constraint. Distances $\mathbf{d}_{i-1}$ and $\mathbf{d}_i$ are highlighted.

However, note that to compute f_i according to equation (1), the knowledge of f_{i-1} is required, and the use of only one FT sensor (as in [7]), does not allow to deal with some DLO configurations. For example, if the DLO is taut on both sides of the gripper, as in the case of *fully constrained* DLO end (see $v_{i,G}$ in Figure 3a), two FT sensors are necessary. Indeed, by measuring f_{i-1} applied by $v_{i-1,G}$, it is possible to compute f_i according to equation (1). In case a gripper is not holding the end of the DLO (as $v_{i-1,G}$ in Figure 3a), f_{i-1} is computed compensating also for the weight of the not tensioned part of DLO, expressed by the term f_{i-2}.
Considering a DLO routed around some pegs as in Figure 3b, we assume tensions f_{i-1} and f_i on the sides of a peg $v_{i,U}$ linked by Capstan equation [25], stating that, in equilibrium, it holds that $f_i = f_{i-1} e^{\mu\gamma}$, where μ is the static friction coefficient, and γ is the angle determined by the contact surface. Assuming μ low, we can consider the tension magnitude constant in the portion of DLO held between the grippers. Indeed, thanks to the use of two FT sensors, it is possible to impose tension on the routed DLO with both grippers, since applying force from only one side does not always guarantee uniform tension across the entire DLO. Moreover, the estimation strategy for *unilateral* and *bilateral* constraints (see Section VI) enables feature points estimation without the need for large motion in the workspace ($\gamma < 145°$). It follows that $s_i < \bar{s}$ for all the e_i between the grippers and that the magnitude of the tension remains almost constant along that portion of DLO. Note that tension transmission along the DLO is not dealt with in [7], while k_i is estimated as detailed in [7].

IV. Force-position based estimators

During the manipulation of the taut DLO, an estimate $\hat{\mathbf{p}}_i$ of the position $\mathbf{p}_i$ of a $v_{i,S}$ $(S = U, B, F)$ has to be computed: Figure 4 shows the possible configurations.

We adopt the same estimation strategy as in [7], namely, using a Kalman filter [26] based on force and position measurements. In fact, [7] considers a case similar to the one shown in Figure 4a, but where $v_{i-2,G}$ is a free hanging point. f_{i-1} can be hence obtained by exploiting only one wrist FT sensor connected to the gripper $v_{i-1,G}$. Defining geometrically $\mathbf{d}_{i-1}$ (see Figure 4a) and setting $\mathbf{d}_{i-1} = \mathbf{0}$, the following observation model is obtained:

$$\mathbf{G}_{i-1}(k)\ \mathbf{p}_{i-1}(k) = \mathbf{G}_{i-1}(k)\ \hat{\mathbf{p}}_i \tag{2}$$

where $\mathbf{G}_{i-1}(k) = \mathbf{f}_{i-1}^{\top}(k)\mathbf{f}_{i-1}(k)\mathbf{I_3} - \mathbf{f}_{i-1}(k)\mathbf{f}_{i-1}^{\top}(k)$ ($\mathbf{I}_n$ denotes the identity $n \times n$ matrix). Following the reasoning detailed in [7], a Kalman filter to estimate $\hat{\mathbf{p}}_i$ can be defined with filter update step at instant k computed as:

$$\hat{\mathbf{p}}_i(k) = \hat{\mathbf{p}}_i^{-}(k) + \mathbf{K}(k)\left(\mathbf{G}_{i-1}(k)\,\mathbf{p}_{i-1}(k) - \mathbf{G}_{i-1}(k)\,\hat{\mathbf{p}}_i^{-}(k)\right) \tag{3}$$

where $\hat{\mathbf{p}}_i^{-}(k)$ is the a priori estimate of the state at step k and $\mathbf{K}(k)$ the Kalman gain. We use this filter to estimate $\hat{\mathbf{p}}_i$ for *fully constrained* end in the configuration of Figure 4a where $\mathbf{f}_{i-1} = \bar{\mathbf{f}}_{sens}^{i-1,G} - \bar{\mathbf{f}}_{sens}^{i-2,G}$: the last two terms are the weight compensated force sensed by the two FT sensors attached to the grippers. The detailed DLO configuration cannot be characterized without the use of both FT sensors.

To estimate $\hat{\mathbf{p}}_i$ for *unilateral* and *bilateral* constraints (Figure 4b), we use similar arguments, introducing $\mathbf{d}_i$. Setting $\mathbf{d}_i = \mathbf{0}$ the following observation model is obtained:

$$\mathbf{G}_i(k)\ \mathbf{p}_{i+1}(k) = \mathbf{G}_i(k)\ \hat{\mathbf{p}}_i \tag{4}$$

where $\mathbf{G}_i(k) = \mathbf{f}_i^{\top}(k)\mathbf{f}_i(k)\mathbf{I_3} - \mathbf{f}_i(k)\mathbf{f}_i^{\top}(k)$. Joining (2) and (4) in a unique observation model, we define a Kalman filter with the filter update step computed as:

$$\hat{\mathbf{p}}_i(k) = \hat{\mathbf{p}}_i^{-}(k) + \mathbf{K}(k)\left(\begin{bmatrix}\mathbf{G}_i(k)\,\mathbf{p}_{i+1}(k)\\ \mathbf{G}_{i-1}(k)\,\mathbf{p}_{i-1}(k)\end{bmatrix} - \begin{bmatrix}\mathbf{G}_i(k)\\ \mathbf{G}_{i-1}(k)\end{bmatrix}\hat{\mathbf{p}}_i^{-}(k)\right) \tag{5}$$

Note that in Figure 4b $v_{i+1,G}$ represents a gripper, while $v_{i-1,S}$ can be a gripper ($S = G$) or a previously estimated contact $S \in \{U, B\}$. $\mathbf{f}_i$ and $\mathbf{f}_{i-1}$ are computed thanks to the measures acquired from the two FT sensors as detailed in Section III, except for their orientations, which are always chosen pointing towards $v_{i,S}$, as in Figure 4b.

For both filters (3) and (5), the initial condition for $\hat{\mathbf{p}}_i$ is placed in the origin of $\{\mathbf{h}_B\}$ with high uncertainty: $\hat{\mathbf{p}}_c^{-}(0) = [0\ 0\ 0]^{\top}$, $\mathbf{P}(0) = \epsilon\,\mathbf{I}_3$, ($\mathbf{P}(k)$ is the covariance matrix of the estimation error).

V. Manipulation Primitives

This Section details the implemented manipulation primitives. Four hybrid force-position primitives, detailed in Figure 5, are defined employing a hybrid force-position control [27]. Moreover, a motion primitive **(E)** *"align y_{EE} with $\mathbf{p}_i$"* is implemented to align the y axis of the EE frame along the direction connecting the TCP position to the position $\mathbf{p}_i$ of a feature. To implement a primitive exploiting hybrid force-position control, a time-varying constraint frame $\{\mathbf{h}_C\}$ must be defined to allow the direct specification of natural constraints ${}^{C}\mathbf{n}$, imposed by the environment, and of artificial constraints ${}^{C}\mathbf{a}$, specifying the desired values of force and position in the task. By considering a robot grasping a DLO, it is possible to manipulate the DLO while keeping it taut by defining a proper $\{\mathbf{h}_C\}$. To specify ${}^{C}\mathbf{n}$ and ${}^{C}\mathbf{a}$, complementary to each other, a selection matrix $\mathbf{\Sigma}$ diagonal with null or unitary element is used, extracting the directions where a natural constraint in velocity applies and an artificial constraint in force can be enforced.

The robotic arms can be controlled separately (individual control) or as a single system (coordinated control), exploiting the concepts of *absolute* and *relative* motion [28]. The absolute motion refers to an *absolute frame* $\{\mathbf{h}_{abs}\}$ defined averaging the positions and orientations of the gripper ones $\{\mathbf{h}_R\}$, $\{\mathbf{h}_L\}$, while the relative motion controls the relative position and orientation of grippers with respect to $\{\mathbf{h}_{abs}\}$.

The velocity commands $\boldsymbol{\zeta}_T$ in Cartesian space are computed according to the hybrid force-position controller as $\boldsymbol{\zeta}_T = \boldsymbol{\zeta}_M + \boldsymbol{\zeta}_F$ where $\boldsymbol{\zeta}_M$ is the motion control signal and $\boldsymbol{\zeta}_F$ the force control one. If individual control is used:

$$\boldsymbol{\zeta}_i = [\dot{\mathbf{x}}_{i,R}\ \ \boldsymbol{\omega}_{i,R}\ \ \dot{\mathbf{x}}_{i,L}\ \ \boldsymbol{\omega}_{i,L}]^{\top}\ \text{ with }\ i = T, M, F \tag{6}$$

otherwise, if coordinate control is selected, it holds:

$$\boldsymbol{\zeta}_i = [\dot{\mathbf{x}}_{i,abs}\ \ \boldsymbol{\omega}_{i,abs}\ \ \dot{\mathbf{x}}_{i,rel}\ \ \boldsymbol{\omega}_{i,rel}]^{\top}\ \text{ with }\ i = T, M, F \tag{7}$$

The linear and angular velocities in $\boldsymbol{\zeta}_M$ are computed as:

$$\dot{\mathbf{x}}_{M,j} = k_p\ {}^{B}_{C}\mathbf{R}\ {}^{C}\mathbf{e}_p \tag{8a}$$

$$\boldsymbol{\omega}_{M,j} = k_o\ {}^{B}_{C}\mathbf{R}\ {}^{C}\mathbf{e}_o \tag{8b}$$

where $j \in \{R, L, abs, rel\}$, k_p and k_o are positive gains and ${}^{B}_{C}\mathbf{R}$ is the rotation matrix between $\{\mathbf{h_C}\}$ and $\{\mathbf{h_B}\}$. ${}^{C}\mathbf{e}_p$ and ${}^{C}\mathbf{e}_o$ are the position and orientation errors, respectively, expressed in constraint frame, comparing desired and current quantities: ${}^{C}\mathbf{e}_p = {}^{C}\mathbf{x}_{d,j} - {}^{C}\mathbf{x}_{c,j}$ and ${}^{C}\mathbf{e}_o$ is computed as explained in [29] exploiting ${}^{C}\mathbf{Q}_{d,j}$ and ${}^{C}\mathbf{Q}_{c,j}$. Given $\mathbf{x}_{c,j}$:

$${}^{C}\mathbf{x}_{c,j} = (\mathbf{I}_3 - \mathbf{\Sigma}_3)\,[{}^{C}_{B}\mathbf{R}\,\mathbf{x}_{c,j} + {}^{C}_{B}\mathbf{t}] \tag{9}$$

where $\mathbf{\Sigma}_3$ are the first three rows of $\mathbf{\Sigma}$, and ${}^{C}_{B}\mathbf{t}$ is the translation vector between $\{\mathbf{h_B}\}$ and $\{\mathbf{h_C}\}$. ${}^{C}\mathbf{Q}_{c,j}$ can be obtained applying the rotation expressed by ${}^{B}_{C}\mathbf{R}^{\top}$ to ${}^{B}\mathbf{Q}_{c,j}$. Since forces must be exerted to tension the DLO, and torques have to be avoided to prevent twisting, in $\boldsymbol{\zeta_F}$ we set $\boldsymbol{\omega}_{F,j} = \mathbf{0}$, while the linear velocities are computed as:

$$\dot{\mathbf{x}}_{F,j} = k_f\ {}^{B}_{C}\mathbf{R}\,({}^{C}\mathbf{f}_{d,j} - {}^{C}\mathbf{f}_{c,j}) \tag{10}$$

where $j \in \{R, L, abs, rel\}$, and k_f can be chosen as the inverse of the estimated elasticity of the DLO. ${}^{C}\mathbf{f}_{d,j}$ is the desired force, while ${}^{C}\mathbf{f}_{c,j}$ is the current force in $\{\mathbf{h}_C\}$:

$${}^{C}\mathbf{f}_{c,j} = \mathbf{\Sigma}_3\,[{}^{C}_{B}\mathbf{R}\,\mathbf{f}_{c,j}] \tag{11}$$

Once $\boldsymbol{\zeta_T}$ is computed, joint velocities are obtained by solving the inverse kinematics problem as explained in [30].

The desired velocities included in ${}^{C}\mathbf{a}$ in Figure 5 can be easily linked to a desired position to be used in equation (8).

VI. Feature points classification and estimation

This Section details a pipeline to manipulate the DLO, classifying the encountered environmental constraints and estimating the poses of the associated frames while updating the graph model: the switch between primitives is controlled based on the estimation results. We assume that the arms initially hold the DLO above the pegs on the worktable in a configuration that permits the robot to apply tension only to the DLO segment between the grippers. First, primitive **(A)** is executed and then it is checked for the presence of *fully constrained* DLO ends by moving back and forth one

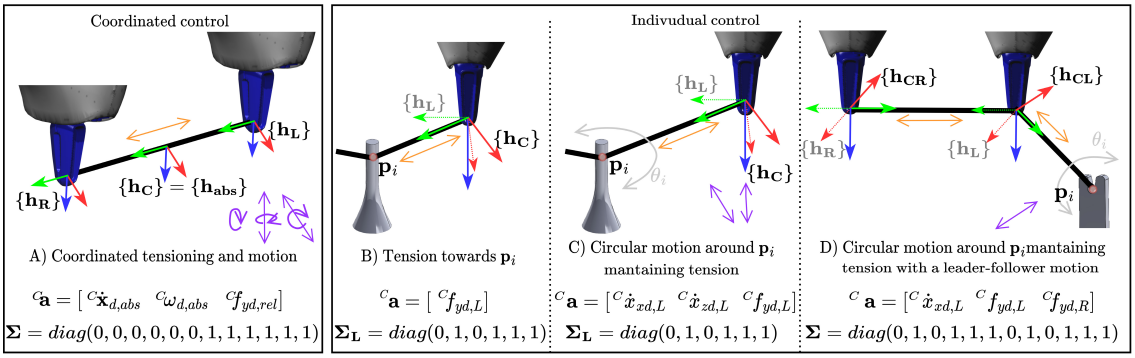

Fig. 5: For each primitive, $\{\mathbf{h}_C\}$ and relevant frames are reported together with the desired values of artificial constraints ${}^C\mathbf{a}$ different from 0, and the selection matrix $\mathbf{\Sigma} \in \mathbb{R}^{12\times12}$ or $\mathbf{\Sigma_L} \in \mathbb{R}^{6\times6}$ if only one arm (i.e. the left one) is controlled. Position and force controlled directions defined by ${}^C\mathbf{a}$ are highlighted in purple and orange, respectively. In **(D)**, a *leader* arm (i.e. the left one) performs a circular motion around a *fully constrained* DLO end, keeping taut the DLO part in between, while the *follower* arm moves to keep the DLO taut between the grippers. Two different constraint frames are used.

Algorithm 1 Motion for estimation of $\mathbf{p}_i$ for a $v_{i,F}$ (*leader* arm: L with gripper defined by $v_{i-1,G}$; *follower* arm: R with gripper defined by $v_{i-2,G}$)

1: $\mathbf{f}_{i-2}^{old} \leftarrow \mathbf{0}$, $\mathbf{f}_{i-2}(k) \leftarrow \mathbf{0}$, $\theta \leftarrow 0$
2: **starting-pose**$(L,R) \leftarrow$ **actual-pose**(L,R)
3: Begin execution of primitive **(D)** with *leader* arm performing a counterclockwise circular motion around $\mathbf{p}_i$ with maximum spanned angle equal to θ_{max}
4: **while** $\theta \leq \theta_{max}$ **do**
5: $\mathbf{f}_{i-2}^{old} \leftarrow \mathbf{f}_{i-2}(k)$
6: Compute $\mathbf{f_{i-2}}(k)$ according to eq. (1) using data from both the FT sensors
7: **if** $\mathbf{f}_{i-2}^{old} \neq \mathbf{0}$ **then**
Check if the DLO is taut from both sides of the *follower* gripper
8: **if** $\alpha = \arccos\left[\frac{\mathbf{f}_{i-2}^{old}\,\mathbf{f}_{i-2}(k)}{||\mathbf{f}_{i-2}^{old}||_2\,||\mathbf{f}_{i-2}(k)||_2}\right] \geq \alpha_{max}$ **then**
9: Stop execution of primitive **(D)**
10: Move to **recovery-pose**(L,R)
11: Go to instruction at line 15
12: **else**
13: **recovery-pose**$(L,R) \leftarrow$ **actual-pose**(L,R)
14: Update θ considering **actual-pose**(L,R) and **starting-pose**(L,R)
15: Repeat from instruction at line 3 but performing a clockwise circular motion

Algorithm 2 Estimation of $\mathbf{p}_i$ for $v_{i,S}$ with $S \in U, B$ (e.g Figure 4b)

1: $\mathbf{p}_i^{old} \leftarrow \mathbf{0}$, $\mathbf{p}_i \leftarrow \mathbf{0}$, $\mathbf{f}_i(k) \leftarrow \mathbf{0}$, $N \leftarrow 0$, Recovery $\leftarrow False$
2: **while** true **do**
3: Compute $\hat{\mathbf{p}}_i(k)$ according to eq. (5) using $\mathbf{f}_{i-1}(k)$ and $\mathbf{f_i}(k)$ (weighted compensated forces sensed by the two FT sensors) and $\mathbf{p}_{i-1}(k)$ and $\mathbf{p}_{i+1}(k)$ (actual grippers positions)
4: Compute the eigenvalues of $\mathbf{P}(k)$: $\lambda_j(k)$, $j = 1,2,3$
Check if the estimate converges and differs from the average between the TCPs
5: **if** $\lambda_j(k) < T_v$ for all $j = 1,2,3$ and $|\hat{\mathbf{p}}_i(k) - \frac{\mathbf{x}_L(k)+\mathbf{x}_R(k)}{2}| \geq T_p$ **then**
6: $N \leftarrow N+1$
7: **else**
8: $N \leftarrow 0$
Check if the estimate has converged and is reliable
9: **if** $N > T_n$ **then**
10: $\mathbf{p}_i^{old} \leftarrow \mathbf{p}_i$, $\mathbf{p}_i \leftarrow \hat{\mathbf{p}}_i(k)$
Check if a new contact is detected
11: **if** $\mathbf{p}_i^{old} \neq \mathbf{0}$ and $|\mathbf{p}_i - \mathbf{p}_i^{old}| > T_{c1}$ **then**
12: Wait until Recovery = $True$ (flag modified in Algorithm 3)
13: Compute $\mathbf{Q}_i$ (and $t_{i,B}, w_{i,B}$ if $v_{i,S}$ is part of a *bilateral* constraint).
14: $i \leftarrow i+1$. Repeat from line 3 using $\mathbf{f}_{i-1}(k) = [-f_{ix}, -f_{iy}, f_{iz}]$, (force propagated along the DLO, with orientation chosen pointing towards the new v_i), $\mathbf{f_i}(k)$ (weighted compensated force sensed by the sensor in v_{i+1}), $\mathbf{p}_{i-1}(k)$ (position of the just estimated contact) and $\mathbf{p_{i+1}}(k)$ (actual gripper position).

arm while the other keeps the DLO taut between the grippers (primitive **(B)**). In particular, if a force different from the one used to tense the DLO is sensed during the motion, then a *fully constrained* end is detected and classified. Subsequently, the robot moves according to Algorithm 1 and the position of the *fully constrained* end (Figure 4a) is estimated using the estimator (3): every time that the estimate $\hat{\mathbf{p}}_i(k)$ converges reliably (the eigenvalues of $\mathbf{P}(k)$ go below a user-defined threshold T_v for at least N consecutive times) $\mathbf{p}_i$ is updated.

Algorithm 3 Motion for estimation of $\mathbf{p}_i$ for $v_{i,S}$ with $S \in U, B$ (arm L with gripper defined by $v_{i+1,G}$; arm R with gripper defined by $v_{i-1,G}$)

1: contact$_1 \leftarrow True$, $t \leftarrow 0$, $\theta \leftarrow 0$,
2: L: Perform primitive **(E)** towards $\mathbf{p}_i$. Perform primitive **(B)** towards $\mathbf{p}_i$
3: **starting-pose**$(L) \leftarrow$ **actual-pose**(L), Recovery $\leftarrow False$, $t \leftarrow k$
4: L: Begin execution of primitive **(C)** performing a circular motion around $\mathbf{p}_i$ with maximum spanned angle equal to θ_{max}
5: **while** $\theta \leq \theta_{max}$ **do**
Check if the DLO has contacted simultaneously two pegs
6: **if** $k - t < W$ and contact$_1$ **then**
7: **if** $\mathbf{p}_i - \mathbf{p}_i^{old} > T_{c2}$ **then**
8: L: Stop execution of Primitive **(C)**, contact$_1 \leftarrow False$
9: R: Perform Primitive **(C)** moving circularly forwards around $\mathbf{p}_i$ of θ_d
10: L: Perform Primitive **(C)** moving circularly backwards around $\mathbf{p}_i$ of θ_d
11: Go to instruction at line 2
12: **else**
13: contact$_1 \leftarrow False$
Check if the estimation has converged and is reliable
14: **if** $N > T_n$ **then**
15: L: Perform primitive **(E)** towards $\mathbf{p}_i$
Check if the estimation is changed
16: **if** $|\mathbf{p}_i - \hat{\mathbf{p}}_i(k)| > T_{c1}$ **then**
17: **recovery-pose**$(L) \leftarrow$ **actual-pose**(L)
Check if a new contact is detected
18: **if** $|\mathbf{p}_i - \mathbf{p}_i^{old}| > T_{c1}$ **then**
19: L: Stop execution of Primitive **(C)**
20: L: Move circularly to **recovery-pose**(L) using Primitive (C)
21: Recovery $\leftarrow True$
22: Repeat from instruction at line 2
23: Update θ considering **actual-pose**(L) and **starting-pose**(L)

If no connected end is detected, Algorithm 2 is activated to estimate possible contacts with pegs enforcing *unilateral/bilateral* constraints. The arms lower the DLO at the height where possible pegs can be contacted and move back and forth, keeping the DLO taut executing primitive **(A)**. If contacts are detected during both the forward and backward motion, a *bilateral* constraint is classified; otherwise, if contact is sensed only from one side, the constraint is *unilateral*. The arms manipulate the DLO estimating and searching for other contacts, routing it in the meanwhile around the estimated contact points exploiting Algorithms 2 and 3. Lines 6 – 7 of Algorithm 3 allow to check if two pegs have been contacted simultaneously during the first point estimation ($\mathbf{p}_i$ changes in a relevant way in a defined time window of width W) and activate a procedure to properly estimate them.

VII. Experimental Validation

The estimation strategy is first validated in a simulated environment based on the physics simulator Algoryx and then on a real setup (Figure 2). A dual-arm ABB YuMi robot,

Parameters:	$T_v = 4$ mm $N = 30$ $T_p = 5$ mm $T_{c1} = 20$ mm $T_{c2} = 15$ mm $\theta_{max} = 60^\circ$ $\alpha_{max} = 5^\circ$ $\theta_d = 20^\circ$ $W = 3$ s $\epsilon = 10$ $\sigma = 0.05$ $q = 10^{-4}$				
Configurations:	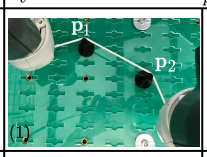	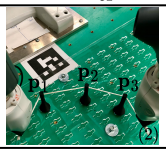	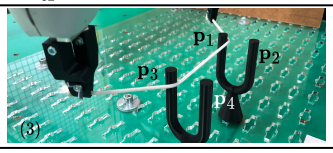	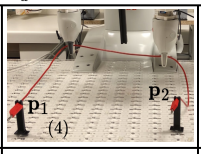	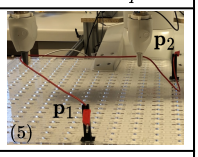
DLO used:	Rope 30cm	Rope 40cm	Rope 30cm	Electric wire 100cm	Electric wire 100cm
Average errors $\bar{\mathbf{e}}_{ij}^{sim}$, $\bar{\mathbf{e}}_{ij}^{rw}$ [mm] Contact i Configuration j	$\bar{\mathbf{e}}_{11}^{sim} = [0.6 \ 1.0 \ 0.4]$ $\bar{\mathbf{e}}_{21}^{sim} = [2.1 \ 2.3 \ 0.2]$ $\bar{\mathbf{e}}_{11}^{rw} = [6.1 \ 5.2 \ 3.2]$ $\bar{\mathbf{e}}_{21}^{rw} = [6.3 \ 3.5 \ 2.5]$	$\bar{\mathbf{e}}_{12}^{sim} = [1.1 \ 2.0 \ 0.9]$ $\bar{\mathbf{e}}_{22}^{sim} = [2.4 \ 2.7 \ 2.4]$ $\bar{\mathbf{e}}_{32}^{sim} = [2.6 \ 2.9 \ 1.9]$ $\bar{\mathbf{e}}_{12}^{rw} = [7.7 \ 11.2 \ 4.3]$ $\bar{\mathbf{e}}_{22}^{rw} = [5.4 \ 8.5 \ 4.0]$ $\bar{\mathbf{e}}_{32}^{rw} = [4.9 \ 4.1 \ 3.1]$	$\bar{\mathbf{e}}_{13}^{sim} = [1.8 \ 3.1 \ 0.4]$ $\bar{\mathbf{e}}_{23}^{sim} = [0.9 \ 2.9 \ 0.4]$ $\bar{\mathbf{e}}_{33}^{sim} = [2.0 \ 1.8 \ 0.3]$ $\bar{\mathbf{e}}_{43}^{sim} = [1.6 \ 1.9 \ 0.2]$ $\bar{\mathbf{e}}_{13}^{rw} = [6.7 \ 4.9 \ 3.6]$ $\bar{\mathbf{e}}_{23}^{rw} = [6.3 \ 5.2 \ 3.3]$ $\bar{\mathbf{e}}_{33}^{rw} = [7.9 \ 5.7 \ 3.5]$ $\bar{\mathbf{e}}_{43}^{rw} = [8.0 \ 5.6 \ 3.8]$	$\bar{\mathbf{e}}_{14}^{sim} = [5.1 \ 3.1 \ 2.0]$ $\bar{\mathbf{e}}_{24}^{sim} = [4.8 \ 2.9 \ 2.3]$ $\bar{\mathbf{e}}_{14}^{rw} = [15.7 \ 16.7 \ 12.9]$ $\bar{\mathbf{e}}_{24}^{rw} = [21.3 \ 14.7 \ 9.9]$	$\bar{\mathbf{e}}_{15}^{sim} = [4.9 \ 4.2 \ 3.2]$ $\bar{\mathbf{e}}_{25}^{sim} = [3.8 \ 3.2 \ 2.9]$ $\bar{\mathbf{e}}_{15}^{rw} = [10.0 \ 14.6 \ 14.5]$ $\bar{\mathbf{e}}_{25}^{rw} = [16.9 \ 14.9 \ 5.7]$

Fig. 6: Parameters used and considered configurations (1 to 5 from left to right). The average errors $\bar{\mathbf{e}}_{i,j}^{sim}$, $\bar{\mathbf{e}}_{i,j}^{rw}$ in [mm] are reported: they are computed by averaging the absolute value of the error of each experiment when the estimate converges until a new contact is encountered and then averaging on all the executed experiments.

equipped with two ATI Mini20 FT sensors, is considered. We test the proposed strategy in five configurations with different DLOs as shown in Figure 6: five experiments are executed for each configuration. The accompanying video shows some of the performed experiments. Figure 6 details the values used for the parameters (q is the process uncertainty and σ the one of the measurements) and of $\bar{\mathbf{e}}_{i,j}^{sim}$, $\bar{\mathbf{e}}_{i,j}^{rw}$ that are the average estimation errors for each $\hat{\mathbf{p}}_i$ in configuration j in simulation and real world, respectively. When routing a DLO, the contact point changes as the contact surface on the peg varies: we use the average position of the contacted surface as ground truth for each contact. As Figure 6 shows, the errors obtained in real world in configuration 2 for $\mathbf{p}_1$ are larger than the ones obtained for $\mathbf{p}_2$ and $\mathbf{p}_3$, in contrast with simulation results. This occurs because, in the real setup, the DLO's considerable length prevents forces from being perfectly aligned along the DLO's shape when contacting just one peg. Longer DLOs require higher amounts of movement to acquire informative force measurements and, in turn, precise contact estimation. As more of the DLO is constrained during the manipulation, force measurements become more informative, enhancing estimation accuracy. Moreover, in the real world, the plastic deformation of the electric wire of configurations 4 and 5 resulted in a non-perfectly linear shape of the taut DLO, bringing worse results than in simulation. The estimation errors in a real world experiment of configuration 1 and in one of configuration 5 are shown in Figures 7 and 8, respectively. Comparing the time histories of the errors shown in these Figures, it is evident that the use of the estimator (5), based on two forces and used for *unilateral/bilateral* constraints, makes the estimate more stable and accurate than the one generated by estimator (3) used for *fully constrained* ends and exploiting only one force obtained subtracting the two sensed forces. The estimation obtained using (5) is good even if the robot does not perform wide motions around the contact, while, in Figure 8, the estimate varies considerably during the motion, since only one force direction is considered in the estimation.

VIII. Conclusions

We consider a dual-arm robot equipped with two wrist FT sensors manipulating a low stiffness DLO in an environment constraining DoFs through contacts. An enhanced graph model for DLOs is presented, containing the semantic representation of environmental constraints. A strategy is proposed to manipulate the tensioned DLO, while classifying and estimating the environmental contacts. The method was successfully tested in real-world experiments, demonstrating that the proposed estimator can enhance its performance by exploiting the redundancy of FT sensors. Future works aim to define a planner for cable routing that concatenates primitives based on the estimation results.

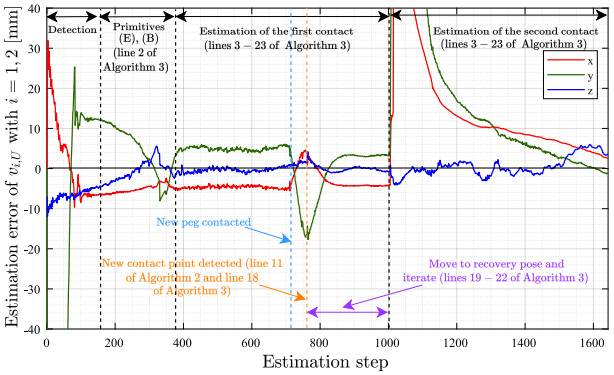

Fig. 7: $\mathbf{e}_i$ [mm] of a real world experiment (configuration 1). At $k = 375$, the left arm starts executing primitive **(C)** around $\mathbf{p}_1$ and the estimate converges. Then, a second peg is contacted at $k = 715$ and the estimation begins to change: as soon as it converges and overcomes T_{c1}, the recovery action is performed, allowing to detach from the new contact: the pose for the first contact is fixed in the online model and, after that, the estimation of the second contact starts.

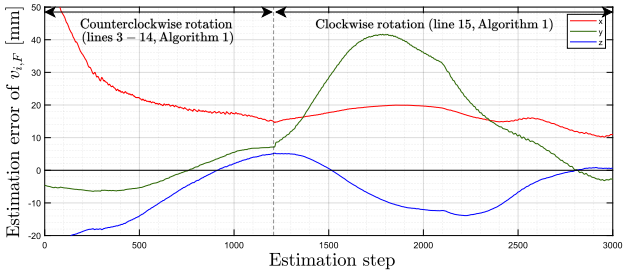

Fig. 8: $\mathbf{e}_i$ [mm] of a real world experiment (configuration 5). The estimation along y changes abruptly when the arms modify the orientation of the rotation: the estimated point is not precise, also due to the considerable length of the DLO between the fixture and the gripper ($\approx$ 30 cm), but primitive **(D)** allows the robot to move and refine the estimation.

REFERENCES

[1] H. Yin, A. Varava, and D. Kragic, "Modeling, learning, perception, and control methods for deformable object manipulation," *Science Robotics*, vol. 6, no. 54, p. eabd8803, 2021.

[2] J. Sanchez, J.-A. Corrales, B.-C. Bouzgarrou, and Y. Mezouar, "Robotic manipulation and sensing of deformable objects in domestic and industrial applications: a survey," *The International Journal of Robotics Research*, vol. 37, no. 7, pp. 688–716, 2018.

[3] S. Jin, W. Lian, C. Wang, M. Tomizuka, and S. Schaal, "Robotic cable routing with spatial representation," *IEEE Robotics and Automation Letters*, vol. 7, no. 2, pp. 5687–5694, 2022.

[4] J. Zhu, B. Navarro, R. Passama, P. Fraisse, A. Crosnier, and A. Cherubini, "Robotic manipulation planning for shaping deformable linear objects withenvironmental contacts," *IEEE Robotics and Automation Letters*, vol. 5, no. 1, pp. 16–23, 2019.

[5] A. Monguzzi, M. Pelosi, A. M. Zanchettin, and P. Rocco, "Tactile based robotic skills for cable routing operations," in *2023 IEEE International Conference on Robotics and Automation (ICRA)*. IEEE, 2023, pp. 3793–3799.

[6] A. Monguzzi, A. M. Zanchettin, and P. Rocco, "Sensorless robotized cable contour following and connector detection," *Mechatronics*, vol. 97, p. 103096, 2024.

[7] F. Süberkrüb, R. Laezza, and Y. Karayiannidis, "Feel the tension: Manipulation of deformable linear objects in environments with fixtures using force information," in *2022 IEEE/RSJ International Conference on Intelligent Robots and Systems (IROS)*. IEEE, 2022, pp. 11 216–11 222.

[8] D. Almeida and Y. Karayiannidis, "Cooperative manipulation and identification of a 2-dof articulated object by a dual-arm robot," in *2018 IEEE International Conference on Robotics and Automation (ICRA)*. IEEE, 2018, pp. 5445–5451.

[9] S. Cruciani, D. Almeida, D. Kragic, and Y. Karayiannidis, "Discrete bimanual manipulation for wrench balancing," in *2020 IEEE International Conference on Robotics and Automation (ICRA)*. IEEE, 2020, pp. 2631–2637.

[10] L. Manuelli and R. Tedrake, "Localizing external contact using proprioceptive sensors: The contact particle filter," in *2016 IEEE/RSJ International Conference on Intelligent Robots and Systems (IROS)*. IEEE, 2016, pp. 5062–5069.

[11] F. Wirnshofer, P. S. Schmitt, P. Meister, G. v. Wichert, and W. Burgard, "State estimation in contact-rich manipulation," in *2019 International Conference on Robotics and Automation (ICRA)*. IEEE, 2019, pp. 3790–3796.

[12] M. Suomalainen, Y. Karayiannidis, and V. Kyrki, "A survey of robot manipulation in contact," *Robotics and Autonomous Systems*, vol. 156, p. 104224, 2022.

[13] Y. Wang, D. Held, and Z. Erickson, "Visual haptic reasoning: Estimating contact forces by observing deformable object interactions," *IEEE Robotics and Automation Letters*, vol. 7, no. 4, pp. 11 426–11 433, 2022.

[14] F. F. Khalil and P. Payeur, "Robotic interaction with deformable objects under vision and tactile guidance-a review," in *2007 International Workshop on Robotic and Sensors Environments*. IEEE, 2007, pp. 1–6.

[15] A. Remde, E. Pfaffenberger, and H. Worn, "Manipulating deformable linear objects-force-based detection of contact state transitions," in *Proceedings. 2000 IEEE/RSJ International Conference on Intelligent Robots and Systems (IROS 2000)(Cat. No. 00CH37113)*, vol. 2. IEEE, 2000, pp. 1480–1486.

[16] A. Schlechter and D. Henrich, "Manipulating deformable linear objects: Characteristics in force signals for detecting contact state transitions," in *Proceedings. 10th International Conference on Advanced Robotics*. IEEE, 2001, pp. 22–25.

[17] Y. Huang, C. Xia, X. Wang, and B. Liang, "Learning graph dynamics with external contact for deformable linear objects shape control," *IEEE Robotics and Automation Letters*, 2023.

[18] J. Sanchez, K. Mohy El Dine, J. A. Corrales, B.-C. Bouzgarrou, and Y. Mezouar, "Blind manipulation of deformable objects based on force sensing and finite element modeling," *Frontiers in Robotics and AI*, vol. 7, p. 73, 2020.

[19] Y. Luo and B. J. Nelson, "Fusing force and vision feedback for manipulating deformable objects," *Journal of Robotic Systems*, vol. 18, no. 3, pp. 103–117, 2001.

[20] A. Cherubini and P. I. Corke, "Towards sensor-based manipulation of flexible objects," in *ICRA Workshop on Sensor-Based Object Manipulation for Collaborative Assembly*, 2017.

[21] B. Kahl and D. Henrich, "Manipulation of deformable linear objects: Force-based simulation approach for haptic feedback," in *ICAR'05. Proceedings., 12th International Conference on Advanced Robotics, 2005.* IEEE, 2005, pp. 115–122.

[22] N. Lv, J. Liu, X. Ding, J. Liu, H. Lin, and J. Ma, "Physically based real-time interactive assembly simulation of cable harness," *Journal of Manufacturing Systems*, vol. 43, pp. 385–399, 2017.

[23] A. Sintov, S. Macenski, A. Borum, and T. Bretl, "Motion planning for dual-arm manipulation of elastic rods," *IEEE Robotics and Automation Letters*, vol. 5, no. 4, pp. 6065–6072, 2020.

[24] X. Jiang, Y. Nagaoka, K. Ishii, S. Abiko, T. Tsujita, and M. Uchiyama, "Robotized recognition of a wire harness utilizing tracing operation," *Robotics and Computer-Integrated Manufacturing*, vol. 34, pp. 52–61, 2015.

[25] Y. Kyosev, *Braiding technology for textiles: Principles, design and processes*. Elsevier, 2014.

[26] R. E. Kalman, "A new approach to linear filtering and prediction problems," *Transaction of the ASME—Journal of Basic Engineering*, pp. 35–45, 1960.

[27] B. Siciliano, L. Sciavicco, L. Villani, and G. Oriolo, *Force control*. Springer, 2009.

[28] P. Chiacchio, S. Chiaverini, and B. Siciliano, "Direct and inverse kinematics for coordinated motion tasks of a two-manipulator system," *ASME Journal of Dynamics, Systems, Measurements, and Control*, vol. 118, pp. 691—-697, 1996.

[29] B. Siciliano, L. Sciavicco, L. Villani, and G. Oriolo, "Differential kinematics and statics," *Robotics: Modelling, Planning and Control*, pp. 105–160, 2009.

[30] G. A. Waltersson, R. Laezza, and Y. Karayiannidis, "Planning and control for cable-routing with dual-arm robot," in *2022 International Conference on Robotics and Automation (ICRA)*. IEEE, 2022, pp. 1046–1052.